Letter

Mechanism of CO Intercalation through the Graphene/Ni(111) Interface and Effect of Doping

Daniele Perilli, Sara Fiori, Mirco Panighel, Hongsheng Liu, Cinzia Cepek, Maria Peressi, Giovanni Comelli, Cristina Africh,* and Cristiana Di Valentin*

Cite This: *J. Phys. Chem. Lett.* 2020, 11, 8887−8892

Read Online

ACCESS | Metrics & More | Article Recommendations | Supporting Information

ABSTRACT: Molecules intercalate at the graphene/metal interface even though defect-free graphene is impermeable to any atomic and molecular species in the gas and liquid phase, except hydrogen. The mechanism of molecular intercalation is still a big open question. In this Letter, by means of a combined experimental (STM, XPS, and LEED) and theoretical (DFT) study, we present a proof of how CO molecules succeed in permeating the graphene layer and get into the confined zone between graphene and the Ni(111) surface. The presence of N-dopants in the graphene layer is found to highly facilitate the permeation process, reducing the CO threshold pressure by more than one order of magnitude, through the stabilization of multiatomic vacancy defects that are the open doors to the bidimensional nanospace, with crucial implications for the catalysis under cover and for the graphene-based electrochemistry.
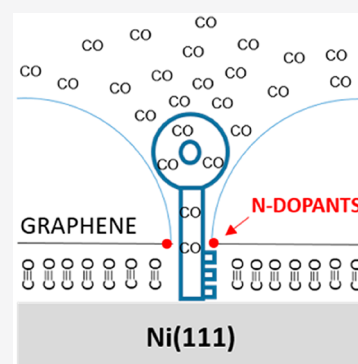
Molecule intercalation at the graphene (Gr)/metal (M) interface is a crucial process for several relevant applications, such as catalysis under cover,[1−3] large-scale preparation of single-layer graphene from chemical vapor deposition (CVD),[4] graphene-based electrochemistry[5] and gas trapping in highly pressurized graphene nanobubbles.[6]

Several experimental proofs exist of the fact that gases succeed in reaching the confined zone beneath Gr.[7−11] For example, scanning tunneling microscopy (STM) images reveal a change in the pattern when the gas intercalation decouples Gr from the substrate.[8] Furthermore, molecular chemical reactivity under graphene is probed by real-time low-energy electron microscopy (LEEM)/photoemission electron microscopy (PEEM), X-ray photoelectron spectroscopy (XPS), and high-resolution electron energy loss (HREELS) spectroscopy.[7,8,12]

However, gas or molecule intercalation still remains mostly an empirical observation: although crucial, the mechanism is not yet understood. It is even not yet established whether it is a general mechanism or it is molecule-dependent. Researchers can prove it occurs, but they do not really know how.

What it is clearly known is that defect-free Gr is impermeable to any atomic or molecular species in gas or liquid phase.[13] Only the permeation of atomic and molecular hydrogen can be activated by the presence of some local curvature, due to a peculiar flipping mechanism, as recently reported.[14] Then, an important open question, which we want to address in the present paper is, provided that G is impermeable, why do researchers observe gas intercalation at Gr/M interfaces?

One may expect that the mechanism of gas intercalation takes place in two main consecutive steps: (1) the gas permeation through the Gr layer; (2) the gas diffusion at the Gr/M interface away from the intercalation sites. The first step is determined by the gas permeability of Gr layers, which has been a topic of intense discussion in the past.[15] The reason is that the ability to precisely control the quantity and location of molecular flux is of value in several graphene applications, such as molecular sieving membranes and sensor design, nanoscale 3D printing, and catalysis.[16,17]

For large-sheet stacked graphene membranes, it has been established that gas permeation may take place by intercalation through structural defects, also known as the inner-sheet pathway, whose kinetics largely depends on their size and concentration.[18] Discrete Ångstrom-sized pores, induced with a voltage pulse applied by a metallized atomic force microscope tip on a single graphene sheet, have also been used to control gas transport and selectivity in molecular valves.[19]

It is reasonable to expect that structural defects play a key role also for the intercalation of gas molecules within Gr/M interfaces, as proposed in a recent experimental work.[5]
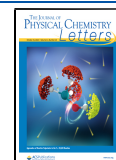
Moreover, a theoretical study suggested that the presence of dopants may influence graphene permeability.[20]

In this work, through a combined theoretical and experimental study, we propose a mechanism of CO intercalation through a Gr/Ni(111) interface, based on density functional theory calculations and consistent with the experimental observations of CO exposure on pristine graphene and N-doped graphene (N-Gr) grown on a Ni(111) surface by low-energy electron diffraction (LEED), XPS, and STM.

High-quality Gr and N-Gr layers on Ni(111) were grown by low-pressure CVD.[21,22] Carbon monoxide was then dosed at pressures in the millibar regime (more details in the experimental section in the Supporting Information). In the LEED patterns obtained for pristine Gr (Figure 1a left), only after exposure to 500 mTorr of CO, new extra spots, besides the Ni and Gr markers, are visible, forming a pattern in line with those reported in literature for CO on clean Ni(111) and compatible with the coexistence of $c(4 \times 2)$ and $(\sqrt{7} \times \sqrt{7})R19°$ CO domains (nominal coverage of 0.5 and 0.57 ML, respectively).[23,24] On the other hand, for N-Gr (Figure 1b left), new spots are present already after exposure to 20 mTorr of CO, yielding one well-defined pattern corresponding to the $(\sqrt{7} \times \sqrt{7})R19°$ CO superstructure on clean Ni (nominal coverage of 0.57 ML).[23,24] On the basis of XPS and STM results, we can rule out that CO is adsorbed on a residual clean Ni region (not covered by Gr or N-Gr), implying that CO intercalation underneath N-Gr occurs at a pressure that is more than one order of magnitude lower than for pristine Gr.

XPS measurements carried out on Gr and N-Gr samples before and after CO exposure (Figure 1a and 1b, right) present features that confirm CO intercalation. In the C 1s spectrum, two new components arise after CO exposure, suggesting a detachment of the layer from the Ni substrate: the first one, at 283.6 eV, is characteristic of C in a G layer decoupled from the metal substrate by intercalated CO;[25] the second one, at 285.3 eV, has been attributed to C in the CO molecule on Ni(111) in the bridge position.[26] The same features are observed in the N-Gr spectrum (Figure 1b right), but already after exposure at significantly lower CO pressure.

We further confirm CO intercalation by STM. In Figure 2a, the atomically resolved Gr layer imaged before CO exposure shows the two triangular sublattices typical of the top-fcc arrangement.[21] Due to the strong Gr/Ni interaction, the C atoms on fcc positions are imaged brighter than those on top, in agreement with density functional theory (DFT) simulations (Figure 2d). In Figure 2b, after CO intercalation below Gr, the whole hexagon of the honeycomb lattice appears with uniform intensity, in agreement with the simulated STM image in Figure 2e. The presence of an intercalated buffer layer affects also the appearance of N-related structures in N-Gr, as evident in Figure 2c for one of the most abundant defects observed on the N-Gr/CO/Ni(111) surface. The bright protrusion at the center is surrounded by a $\sqrt{3} \times \sqrt{3}$ pattern, not present before CO intercalation,[22] which we ascribe to the typical quantum interference pattern due to scattering by one or more C vacancies in a Gr layer that is weakly interacting with the substrate.[27] This defect is a 3N pyridinic species, as unambiguously confirmed by the simulated STM image in Figure 2f.

Thus, the morphological and chemical characterization of pristine Gr and N-Gr yields very similar results with all the applied techniques (both at the atomic scale with STM as well
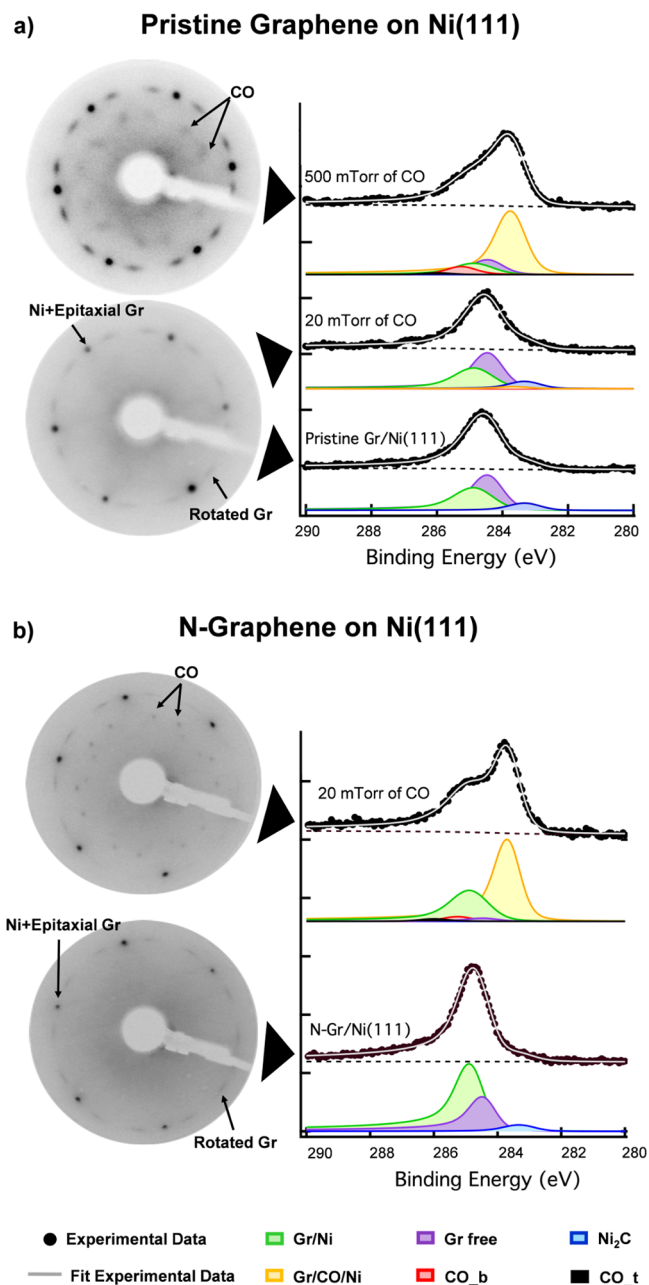
Figure 1. LEED patterns and XPS spectra of (a) pristine Gr and (b) N-Gr on Ni(111) substrates before and after CO exposure in the millibar regime. The colors of the different XPS components correspond to: green, Gr interacting with Ni; purple, Gr not interacting with Ni (Ni carbide underneath Gr); blue, Ni carbide; yellow, Gr interacting with CO (CO underneath Gr); red and black, CO on Ni(111) in bridge and top positions, respectively.

as by integrating methods like LEED and XPS), with the only crucial difference being the threshold pressure required to induce CO intercalation and Gr decoupling: 500 mTorr vs 20 mTorr, respectively.

The next question to answer is how did CO molecules get through the graphene layer and reach the Gr/Ni(111) interface? Since even H_2, the smallest molecule in nature, cannot penetrate directly through the center of the C hexagon, graphene must be impermeable to CO molecules. Therefore, reasonably, there must be some vacancies in the graphene lattice. How big should these "holes" be to allow a CO
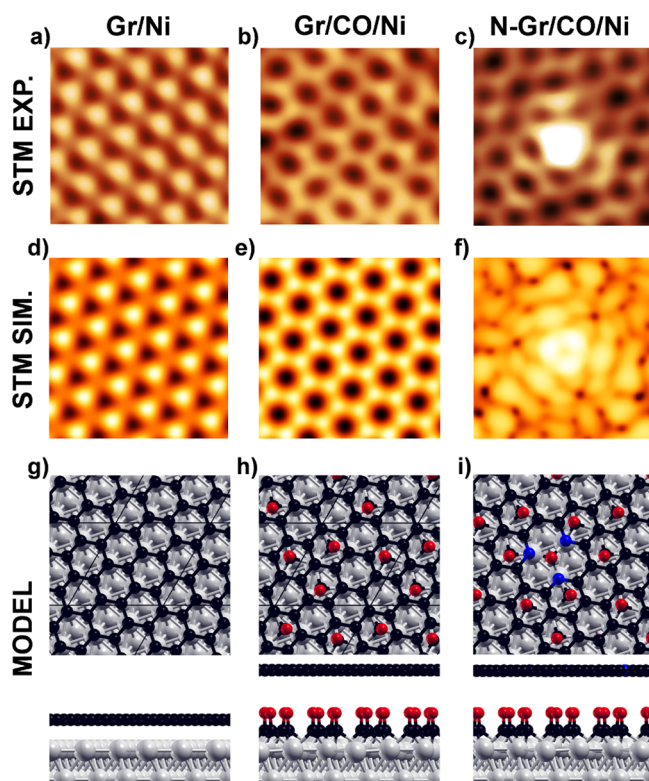
Figure 2. Pristine and N-doped Gr/Ni interfaces with and without intercalated CO molecules at 0.57 ML coverage. Experimental (panels a–c) and DFT simulated (panels d–f) STM images. Image size: 1.2 × 1.2 nm^2. Experimental parameters: (a) I = 0.1 nA, V_{bias} = −0.3 V; (b) I = 0.7 nA, V_{bias} = −0.2 V; (c) I = 0.98, nA V_{bias} = −0.05 V. Computational parameters: (d, e) V_{bias} = −0.2 V, ILDOS isosurface lying at 2 Å above graphene; (f) V_{bias} = −0.05 V, ILDOS iso-surface lying ≈3 Å above graphene and with ILDOS value of 1×10^{-5} |e|/a_0^3. Panels (g)−(i): ball-and-stick models of the DFT relaxed structures (top and side views). Color coding: Ni atoms in gray, C atoms in black, O atoms in red, and N atoms in blue.

molecule to pass? Then, why is it so much easier to reach the interface when Gr is doped with N?

The most common atomic defect in pristine Gr/Ni(111) is known to be a triatomic C vacancy trapping a Ni adatom (1Ni@3VG).[28] However, this seems not to be the gate for intercalation: if we model a CO molecule on top of it, the C atom is found to fill one of the vacancies whereas O becomes very tightly bound to Ni. When we add a second CO molecule, we observe the formation of CO_2 with one C left in the defect (Figure S1). In the case of N-Gr/Ni(111), the most common atomic defect is a C monovacancy surrounded by three pyridinic N atoms, as discussed above.[22] The adsorption of one CO in this C vacancy is however very unstable (by ∼3 eV), because the defect is too small to accommodate it (Figure S2).

Therefore, one crucial aspect for the CO permeation through the graphene layer appears to be the critical size of the atomic holes allowing the molecules to pass through. Since the triatomic vacancy is found not to be suitable, we have investigated a tetra-atomic vacancy. The undercoordinated C atoms surrounding the vacancy are very reactive and therefore either they bind to the underlying Ni substrate, blocking the passage of the molecules into the confined zone between the Gr and the Ni(111) surface,[29] or they might react with residual hydrogen gas present in the chamber forming CH bonds[30] or directly with the dosed CO molecules. These reactions yield

the two configurations shown in Figure 3a and b. Instead, for the case of defective N-Gr, we have found that N atoms tend
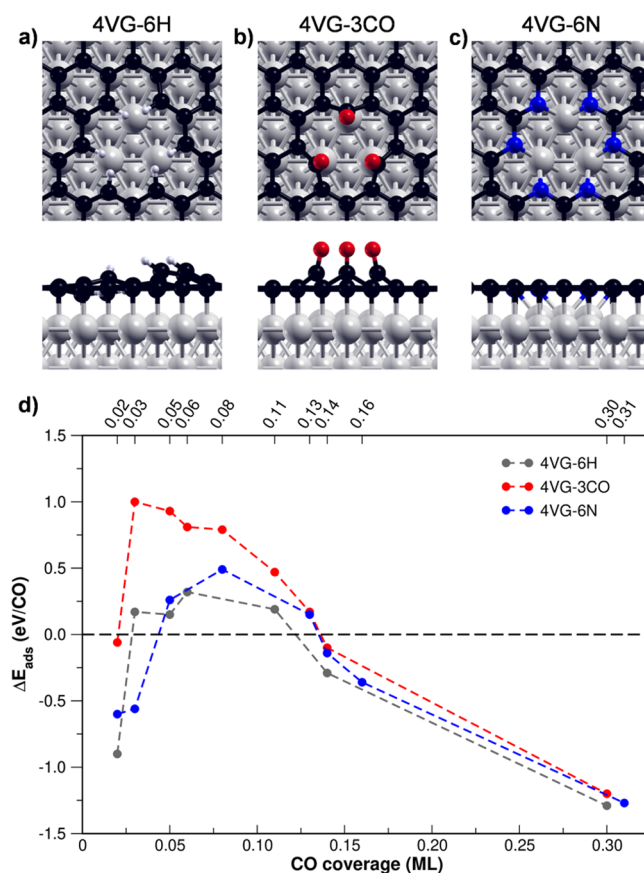
Figure 3. Top and side views for the three models of vacancy considered: (a) 4VG-6H, (b) 4VG-3CO, and (c) 4VG-6N. Color coding: Ni atoms in gray, C atoms in black, H atoms in light gray, O atoms in red, and N atoms in blue. (d) Energy profile (normalized by the number of CO molecules) for the CO adsorption as a function of the CO coverage for each of the vacancy models: 4VG-6H, 4VG-3CO, and 4VG-6N (gray, red, and blue line, respectively). Values of the coverages represented by the dots in the curves are reported on the top x-axis. The ball-and-stick representations of the structures at different CO coverage for 4VG-6N are shown in Figure S4.

to diffuse and segregate to the defect edges, where they become pyridinic.[22] In other words, there is a downhill slope in energy, which favors the concentration of pyridinic N at the defect edges, passivating the defect toward reactivity with H_2 or CO. By simply comparing the structures of the three types of holes in Figure 3a−c (4VG-6H, 4VG-3CO, and 4VG-6N), there is an evident obstruction of the hole for 4VG-3CO, whereas 4VG-6N appears to be the largest, with no steric hindrance. Moreover, the N atoms at the edges are much less strongly bound to the underlying Ni substrate than unsaturated C atoms.

We will focus the attention on the 4VG-3CO and 4VG-6N models, which, at variance with the 4VG-6H model, do not require dissociation of gas phase molecules for their formation. More specifically, we have investigated the energy profile for one CO molecule to vertically enter the atomic hole, by moving the CO molecule along the z-direction and, at each different CO height, allowing all the atoms to fully relax. The two energy profiles for 4VG-3CO and for 4VG-6N, reported in

Figure S3, are extremely different: for 4VG-3CO, the energy goes up to almost 5 eV when the distance of CO from the Ni surface is 2.6 Å, whereas for 4VG-6N it reaches a value of only 0.19 eV, which represents a rough estimation of the activation barrier. On this basis, we can draw an important conclusion: N-doping causes a chemical stabilization of multivacancies in Gr, which results in much less sterically hindered atomic holes in the 2D network, thus facilitating molecule permeation. We expect this to have a tremendous effect on the threshold pressure for CO intercalation, as we will discuss in the following.

For both 4VG-3CO and 4VG-6N, our calculations show that the first CO molecule is favorably bound to the Ni surface, by -0.06 and -0.60 eV, respectively. As a further step in our mechanistic study, we have added other CO molecules, one at a time, and analyzed the variation in energy as normalized to the number of added CO molecules (see Figure 3d). We did this for all the three "hole" models. The three curves are quite different in the first part of the graph, but they tend to line up in the second part, above 0.11 ML. 4VG-6N presents an energy profile which never exceeds 0.5 eV and is very similar to the one of 4VG-6H, where we do not expect any strong interaction of the CH groups with the underlying Ni substrate. This means that, for 4VG-6N, it is not too energetically demanding for one CO molecule at a time not only to go through the hole (see Figure S3), but also to intercalate in the confined zone between the Gr layer and the Ni surface (see Figure 3d). This is because the N atoms are not strongly interacting with the substrate and therefore can be lifted at a reasonable cost to facilitate the CO passage. All the structures at different CO coverages for 4VG-6N are shown in Figure S4. The highest energy value ($\sim$0.5 eV) is registered at 0.08 ML coverage, then the curve starts to slope down. Very interestingly, at the turn between 0.13 and 0.14 ML, we observe an inversion in the energy, going to negative values. In other words, from 0.14 ML onward, there is an energy gain for each additional CO molecule. This twist is actually observed at 0.14 ML for all the models of multivacancy considered, thus suggesting that something special occurs at this coverage.

Some important insight on this issue comes from a similar analysis, performed for a nondefective Gr layer on the Ni(111) substrate and reported in Figure S5. Even in this case, where no defect is present in the Gr lattice, we observe that the cost to have CO molecules in the confined zone between the two materials reduces with the number of added molecules, turning into an energy gain for coverages $\geq$ 0.14 ML. Therefore, 0.14 ML corresponds to the critical point when the cost to detach the Gr layer from the Ni substrate is counterbalanced and even overcome by the gain of establishing a certain amount of Ni–CO bonds.

We have performed an energy decomposition analysis for 4VG-6N to establish the exact contributions from (1) the cost to decouple Gr/Ni(111) (ΔE_{decoup}); (2) the cost to distort Gr/Ni(111) to accommodate the CO molecules (ΔE_{dist}); (3) the binding energy for the Ni–CO bonds (ΔE_{bind}). The first two terms are energy costs, whereas the third one is an energy gain, as shown in Figure 4 and detailed in Table 1. We carried out this analysis at the two critical coverages where there is an inversion in the energy balance: gain/cost at 0.03/0.05 ML and cost/gain at 0.13/0.14 ML (see Figure 3d). We observe that going from 0.03 to 0.05 ML there is a large increase in the energy cost of distortion (+1.02 eV/CO) but a small reduction in the cost for decoupling (-0.15 eV/CO), whereas the energy
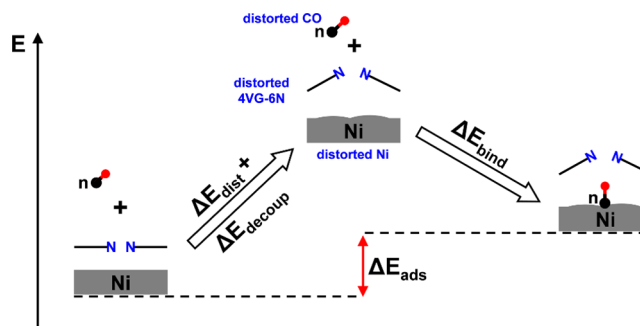
Figure 4. Schematic representation of the energy decomposition analysis for the energy contribution of distortion (positive, ΔE_{dist}), decoupling (positive, ΔE_{decoup}), and binding (negative, ΔE_{bind}) to the adsorption energy (ΔE_{ads}) of CO at the interface between N-doped graphene (4VG-6N) and Ni(111) surface. All the energy contributions are normalized by the number of CO molecules.

Table 1. Energy Contributions of the Energy Decomposition Analysis for CO Adsorption on 4VG-6N of Distortion (Positive, ΔE_{dist}), Decoupling (Positive, ΔE_{decoup}), and Binding (Negative, ΔE_{bind}) to the Adsorption Energy (ΔE) at Different CO Coverages[a]

| CO coverage (ML)	ΔE_{ads} (eV/CO)	ΔE_{dist} (eV/CO)	ΔE_{decoup} (eV/CO)	ΔE_{bind} (eV/CO)
0.03	-0.56	$+0.43$	$+0.59$	-1.58
0.05	$+0.26$	$+1.45$	$+0.44$	-1.63
		$+1.02$	-0.15	-0.05
0.13	$+0.15$	$+0.08$	$+2.66$	-2.59
0.14	-0.14	$+0.04$	$+2.42$	-2.61
		-0.04	-0.24	-0.02

[a]All terms are normalized to the number of CO molecules (eV/CO). Total energy differences are reported in Table S1. The energy contributions are calculated using as a reference the optimized 4VG-6N interface and isolated CO molecules in the gas-phase.

gain due to CO binding per molecule is about the same (difference of only -0.05 eV/CO). On the contrary, going from 0.13 to 0.14 ML, we observe a small decrease both in the energy cost of distortion (-0.04 eV/CO) and of decoupling (-0.24 eV/CO) with a similar energy gain of binding per CO molecule (-0.02 eV/CO).

Another important aspect of the intercalation mechanism is related to the role played by the CO molecules distribution on the surface. We assumed that in the initial phase most of the CO molecules are close to the multiatomic hole through which they have reached the Ni surface; then, they gradually diffuse under the Gr layer and become more equally distributed on the surface. We have verified that this picture is compatible with the energy costs involved. First, we have compared the stabilization energy at 0.14 ML for two different CO distributions for 4VG-6N, as shown in Figure S6: (a) close to the hole edges and (b) more equally distributed beneath graphene, at the interface. From (a) to (b), there is an energy gain per CO molecule of -0.044 eV ($\times$9 CO = -0.40 eV), which indicates a driving force for the CO molecules to disperse, reducing their repulsive interaction. We estimated the activation barrier for the CO diffusion in the confined zone between Ni(111) and Gr through a nudged elastic band (NEB) calculation to be 0.19 eV (Figure S7), which is very close to that computed for the corresponding process on the

bare Ni(111) surface, experimentally observed already at 130 K, which is 0.15 eV.[31,32]

Finally, we prove by means of STM that defects with a size comparable to 4VG are rare in pristine Gr whereas they are often visualized on the N-Gr surface, both at the grain boundaries and within the N-Gr domains. Figure 5a reports an
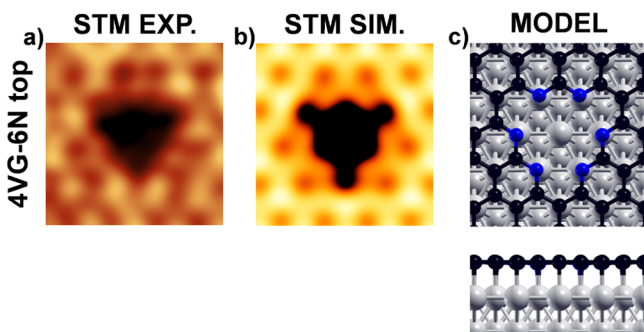
Figure 5. (a) Experimental and (b) simulated STM images of the 4VG-6N top configuration. (c) Ball-and-stick model in top and side views. Experimental parameters: (a) I = 1.4 nA, V_{bias} = −0.2 V. Computational parameters: V_{bias} = −0.2 V; ILDOS iso-surface lying ≈2 Å above graphene and with ILDOS value of 5×10^{-5} |e|/a_0^3. Color coding: Ni atoms in gray, C atoms in black, and N atoms in blue.

atomic scale image of a typical large defect present on the N-Gr/Ni(111) layer. It appears as a big dark triangular feature, which suggests a multiatomic vacancy. This large defect is remarkably well reproduced by the simulated STM image of a tetra-atomic vacancy with edges decorated by six N atoms in the top positions (Figure 5b), thus differing from the 4VG-6N model proposed above only for the registry with the substrate.

In conclusion, our work, based on the synergic contribution of DFT calculations and LEED, XPS, and STM experiments, has unraveled and given proof of the mechanism of CO intercalation at the Gr/Ni interface, which is highly facilitated by the presence of N-dopants, stabilizing multiatomic vacancy defects and turning them in narrow open doors to the confined zone between the two materials. Similar mechanisms are likely to apply to other cases of molecular intercalation at the Gr/M interface, where the process has been observed but not yet explained. The next challenge is to assess to what extent the mechanism we have proposed is a general one, which will require a systematic investigation considering other gases and different dopants. A clear solution to this puzzle is a crucial step toward engineering the Gr/M interface in order to design and realize systems with tailored properties for practical applications.

ASSOCIATED CONTENT

Ⓢ Supporting Information

The Supporting Information is available free of charge at https://pubs.acs.org/doi/10.1021/acs.jpclett.0c02447.

> Computational details, experimental details, reaction path of CO at 1Ni@3VG, models of CO adsorption of 3N^{pyr}, energy profile of CO approaching 4VG-3CO and 4VG-6N, models of intercalated CO in 4VG-6N at different CO coverage, energy profile of intercalated CO in Gr/Ni(111) at different CO coverage, two different CO distributions at 0.14 ML for 4VG-6N, energy profile

for CO diffusion in the Gr/Ni(111) interface, energy decomposition analysis based on total energies (PDF)

AUTHOR INFORMATION

Corresponding Authors

Cristina Africh − *CNR-IOM, Laboratorio TASC, 34149 Trieste, Italy;* ⓞ orcid.org/0000-0002-1922-2557; Email: africh@iom.cnr.it

Cristiana Di Valentin − *Dipartimento di Scienza dei Materiali, Università di Milano-Bicocca, I-20125 Milano, Italy;* ⓞ orcid.org/0000-0003-4163-8062; Email: cristiana.divalentin@unimib.it

Authors

Daniele Perilli − *Dipartimento di Scienza dei Materiali, Università di Milano-Bicocca, I-20125 Milano, Italy*

Sara Fiori − *Department of Physics, University of Trieste, 34127 Trieste, Italy; CNR-IOM, Laboratorio TASC, 34149 Trieste, Italy*

Mirco Panighel − *CNR-IOM, Laboratorio TASC, 34149 Trieste, Italy*

Hongsheng Liu − *Dipartimento di Scienza dei Materiali, Università di Milano-Bicocca, I-20125 Milano, Italy; Laboratory of Materials Modification by Laser, Ion and Electron Beams, Dalian University of Technology, Ministry of Education, Dalian 116024, China*

Cinzia Cepek − *CNR-IOM, Laboratorio TASC, 34149 Trieste, Italy*

Maria Peressi − *Department of Physics, University of Trieste, 34127 Trieste, Italy;* ⓞ orcid.org/0000-0001-6142-776X

Giovanni Comelli − *Department of Physics, University of Trieste, 34127 Trieste, Italy; CNR-IOM, Laboratorio TASC, 34149 Trieste, Italy;* ⓞ orcid.org/0000-0003-4603-2094

Complete contact information is available at:
https://pubs.acs.org/10.1021/acs.jpclett.0c02447

Author Contributions

D.P. and S.F. have contributed equally to this work.

Notes

The authors declare no competing financial interest.

ACKNOWLEDGMENTS

REFERENCES

(1) Jin, L.; Fu, Q.; Dong, A.; Ning, Y.; Wang, Z.; Bluhm, H.; Bao, X. Surface chemistry of CO on Ru (0001) under the confinement of graphene cover. *J. Phys. Chem. C* **2014**, *118*, 12391−12398.

(2) Fu, Q.; Bao, X. Surface chemistry and catalysis confined under two-dimensional materials. *Chem. Soc. Rev.* **2017**, *46*, 1842−1874.

(3) Li, H.; Xiao, J.; Fu, Q.; Bao, X. Confined catalysis under two-dimensional materials. *Proc. Natl. Acad. Sci. U. S. A.* **2017**, *114*, 5930−5934.

(4) Ma, D.; Zhang, Y.; Liu, M.; Ji, Q.; Gao, T.; Zhang, Y.; Liu, Z. Clean transfer of graphene on Pt foils mediated by a carbon monoxide intercalation process. *Nano Res.* **2013**, *6*, 671−678.

(5) Palacio, I.; Otero-Irurueta, G.; Alonso, C.; Martínez, J. I.; López-Elvira, E.; Muñoz-Ochando, I.; Salavagione, H. J.; López, M. F.;

García-Hernandez, M.; Méndez, J.; Ellis, G. J.; Martín Gago, J. A. Chemistry below graphene: Decoupling epitaxial graphene from metals by potential-controlled electrochemical oxidation. *Carbon* **2018**, *129*, 837−846.

(6) Zahra, K. M.; Byrne, C.; Alieva, A.; Casiraghi, C.; Walton, A. S. Intercalation, decomposition, entrapment-a new route to graphene nanobubbles. *Phys. Chem. Chem. Phys.* **2020**, *22*, 7606−7615.

(7) Mu, R.; Fu, Q.; Jin, L.; Yu, L.; Fang, G.; Tan, D.; Bao, X. Visualizing chemical reactions confined under graphene. *Angew. Chem., Int. Ed.* **2012**, *51*, 4856−4859.

(8) Granas, E.; Andersen, M.; Arman, M. A.; Gerber, T.; Hammer, B.; Schnadt, J.; Andersen, J. N.; Michely, T.; Knudsen, J. CO intercalation of graphene on Ir (111) in the millibar regime. *J. Phys. Chem. C* **2013**, *117*, 16438−16447.

(9) Wei, M.; Fu, Q.; Yang, Y.; Wei, W.; Crumlin, E.; Bluhm, H.; Bao, X. Modulation of surface chemistry of CO on Ni (111) by surface graphene and carbidic carbon. *J. Phys. Chem. C* **2015**, *119*, 13590−13597.

(10) Silva, C. C.; Cai, J.; Jolie, W.; Dombrowski, D.; Farwick zum Hagen, F. H.; Martínez-Galera, A. J.; Schlueter, C.; Lee, T.-L.; Busse, C. Lifting Epitaxial Graphene by Intercalation of Alkali Metals. *J. Phys. Chem. C* **2019**, *123*, 13712−13719.

(11) Petrović, M.; Rakić, I. Š.; Runte, S.; Busse, C.; Sadowski, J. T.; Lazić, P.; Pletikosić, I.; Pan, Z.-H.; Milun, M.; Pervan, P.; Atodiresei, N.; Brako, R.; Šokčević, D.; Valla, T.; Michely, T.; Kralj, M. The mechanism of caesium intercalation of graphene. *Nat. Commun.* **2013**, *4*, 2772.

(12) He, G.; Wang, Q.; Yu, H. K.; Farías, D.; Liu, Y.; Politano, A. Water-induced hydrogenation of graphene/metal interfaces at room temperature: Insights on water intercalation and identification of sites for water splitting. *Nano Res.* **2019**, *12*, 3101−3108.

(13) Bunch, J. S.; Verbridge, S. S.; Alden, J. S.; Van Der Zande, A. M.; Parpia, J. M.; Craighead, H. G.; McEuen, P. L. Impermeable atomic membranes from graphene sheets. *Nano Lett.* **2008**, *8*, 2458−2462.

(14) Sun, P. Z.; Yang, Q.; Kuang, W. J.; Stebunov, Y. V.; Xiong, W. Q.; Yu, J.; Nair, R. R.; Katsnelson, M. I.; Yuan, S. J.; Grigorieva, I. V.; Lozada-Hidalgo, M.; Wang, F. C.; Geim, A. K. Limits on gas impermeability of graphene. *Nature* **2020**, *579*, 229−232.

(15) Yoon, H. W.; Cho, Y. H.; Park, H. B. Graphene-based membranes: status and prospects. *Philos. Trans. R. Soc., A* **2016**, *374*, 20150024.

(16) Kim, H. W.; Yoon, H. W.; Yoon, S.-M.; Yoo, B. M.; Ahn, B. K.; Cho, Y. H.; Shin, H. J.; Yang, H.; Paik, U.; Kwon, S.; Choi, J.-Y.; Park, H. B. Selective gas transport through few-layered graphene and graphene oxide membranes. *Science* **2013**, *342*, 91−95.

(17) Pierleoni, D.; Minelli, M.; Ligi, S.; Christian, M.; Funke, S.; Reineking, N.; Morandi, V.; Doghieri, F.; Palermo, V. Selective gas permeation in graphene oxide-polymer self-assembled multilayers. *ACS Appl. Mater. Interfaces* **2018**, *10*, 11242−11250.

(18) Ibrahim, A.; Lin, Y. S. Gas permeation and separation properties of large-sheet stacked graphene oxide membranes. *J. Membr. Sci.* **2018**, *550*, 238−245.

(19) Wang, L.; Drahushuk, L. W.; Cantley, L.; Koenig, S. P.; Liu, S.; Pellegrino, J.; Strano, M. S.; Bunch, J. S. Molecular valves for controlling gas phase transport made from discrete ångström-sized pores in graphene. *Nat. Nanotechnol.* **2015**, *10*, 785−790.

(20) Mallineni, S. S. K.; Boukhvalov, D. W.; Zhidkov, I. S.; Kukharenko, A. I.; Slesarev, A. I.; Zatsepin, A. F.; Cholakh, S. O.; Rao, A. M.; Serkiz, S. M.; Bhattacharya, S.; Kurmaev, E. Z.; Podila, R. Influence of dopants on the impermeability of graphene. *Nanoscale* **2017**, *9*, 6145−6150.

(21) Bianchini, F.; Patera, L. L.; Peressi, M.; Africh, C.; Comelli, G. Atomic scale identification of coexisting graphene structures on Ni (111). *J. Phys. Chem. Lett.* **2014**, *5*, 467−473.

(22) Fiori, S.; Perilli, D.; Panighel, M.; Cepek, C.; Ugolotti, A.; Sala, A.; Liu, H.; Comelli, G.; Di Valentin, C.; Africh, C. "Inside Out" Growth Method for High-Quality Nitrogen-Doped Graphene. *Carbon* **2021**, *171*, 704−710.

(23) Campuzano, J. C.; Dus, R.; Greenler, R. G. The sticking probability, dipole moment, and absolute coverage of CO on Ni (111). *Surf. Sci.* **1981**, *102*, 172−184.

(24) Erley, W.; Besocke, K.; Wagner, H. Absolute coverage determination of CO on Ni (111). *J. Chem. Phys.* **1977**, *66*, 5269−5273.

(25) Wei, M.; Fu, Q.; Yang, Y.; Wei, W.; Crumlin, E.; Bluhm, H.; Bao, X. Modulation of surface chemistry of CO on Ni (111) by surface graphene and carbidic carbon. *J. Phys. Chem. C* **2015**, *119*, 13590−13597.

(26) Held, G.; Schuler, J.; Sklarek, W.; Steinrück, H. P. Determination of adsorption sites of pure and coadsorbed CO on Ni (111) by high resolution X-ray photoelectron spectroscopy. *Surf. Sci.* **1998**, *398*, 154−171.

(27) Mallet, P.; Varchon, F.; Naud, C.; Magaud, L.; Berger, C.; Veuillen, J. Y. Electron states of mono-and bilayer graphene on SiC probed by scanning-tunneling microscopy. *Phys. Rev. B: Condens. Matter Mater. Phys.* **2007**, *76*, 041403.

(28) Carnevali, V.; Patera, L. L.; Prandini, G.; Jugovac, M.; Modesti, S.; Comelli, G.; Peressi, M.; Africh, C. Doping of epitaxial graphene by direct incorporation of nickel adatoms. *Nanoscale* **2019**, *11*, 10358−10364.

(29) Dong, A.; Fu, Q.; Wu, H.; Wei, M.; Bao, X. Factors controlling the CO intercalation of h-BN overlayers on Ru (0001). *Phys. Chem. Chem. Phys.* **2016**, *18*, 24278−24284.

(30) Patera, L. L.; Bianchini, F.; Troiano, G.; Dri, C.; Cepek, C.; Peressi, M.; Africh, C.; Comelli, G. Temperature-driven changes of the graphene edge structure on Ni (111): Substrate vs hydrogen passivation. *Nano Lett.* **2015**, *15*, 56−62.

(31) Zhu, X. D.; Rasing, T.; Shen, Y. R. Surface diffusion of CO on Ni (111) studied by diffraction of optical second-harmonic generation off a monolayer grating. *Phys. Rev. Lett.* **1988**, *61*, 2883.

(32) Lin, T. S.; Lu, H. J.; Gomer, R. Diffusion of CO on Ni (111) and Ni (115). *Surf. Sci.* **1990**, *234*, 251−261.